Cell Reports
Physical Science

CellPress

Surpassing the Strength of Metallogels with a Rigid Amorphous Metal-Rich Material Formulation

James Armstrong,[1] Patrick Shea,[2] Cameron C. Cornell,[2] Taylor Bryson,[2] Harris E. Mason,[2] Keith D. Morrison,[2] Marcus Tofanelli,[3] James P. Lewicki,[2] Brandon C. Wood,[2] Bradley F. Guilliams,[1] W. Scott Compel,[3,*] and Christopher J. Ackerson, [1,4,**]

[1]Department of Chemistry, Colorado State University, Fort Collins, CO, USA
[2]Lawrence Livermore National Laboratory, Livermore, CA, USA
[3]AEMS Corp. Livermore, CA, USA
[4]Lead Contact
*Correspondence: scott@aemscorp.com
**Correspondence: chris.ackerson@colostate.edu

SUMMARY

Metal ion containing soft materials include metallogels, metal-organic frameworks, and coordination polymers. These materials show commercial value in catalysis, hydrogen storage, and electronics. All metal-containing soft materials reported to date are structurally weak, falling short of a Young's modulus typical of engineering grade materials. We report herein that inclusion of an antisolvent in metal-thiolate metallogel synthesis results in a colloidal sol, where the colloids comprise amorphous metal-organic complexes. Upon desolvation, the colloids coalesce to form a solid phase that is both gel-like and glass-like. This solid phase is structurally amorphous, comprises continuous networks similar to organic polymers, and has stiffness observed in polymeric materials with extended structure, yet contains a superstoichiometric amount of metal relative to organic ligand. The solid phase is therefore a Rigid Amorphous Metal-Rich (RAMETRIC) material. Highlighting the rigidity, the Young's modulus of gel-phase material is 1000X greater than metallogels comprised of the same constituent building blocks.

Metallogels; Colloids; Sol-Gel Transition; Metal-organic complexes.

INTRODUCTION

Incorporation of metals into soft materials weds the magnetic, optical, and catalytic properties of metals to the tunable mechanical behavior of soft materials.[1–3] The nano- and microstructures of these materials are defined at the nanoscale by the bonding geometries unique to metal-ligand chemistry.[4,5] Metallosupramolecular assemblies, coordination polymer networks, and metal-organic frameworks are all composed of cationic metal nodes bound to organic ligands to frame a molecular architecture.[1,6,7] Judicious selection of organic ligands in conjunction with a metal's preferred coordination environment enables rational design.[8,9]

Coinage metals (Au, Ag, Cu) are well-known to bind to thiols (HSR) to form metallopolymer hydrogels with 1:1 M(I):SR stoichiometry.[10–12] These coinage metal-thiolate polymers (CMTPs) assemble into 1-D chains[13–15] or laterally into 2-D crystalline sheets, generally as hydrogels.[4,5,10,16] The 2-D sheets often stack in the third dimension, forming fibers that entangle and trap solvent to form "metallophilic" hydrogels (metallogels).[11,12] Silver-cysteine (Ag-cys) hydrogels are highly desirable for their antibiotic properties, but they are structurally weak materials that often require adsorption onto other more rigid substrates for successful application.[4,17]

Compared to gels (and other metal-containing soft materials), synthetic polymers are much stronger materials. This can be attributed to the continuous and entangled networks of strong covalent bonds. Incorporation of metals in polymer materials typically compromises their structural integrity, producing weaker materials at higher metal content.

Here, we report a soft-material with both high metal content and polymer-like rigidity. The material is comprised of Ag and cysteine. The inclusion of an antisolvent (diglyme) during the mixing of Ag and cysteine causes the Ag and cysteine to form a colloidal sol comprised of ~50 nm particles. In the absence of diglyme, a previously described metallogel comprised of stacked sheets forms.[16] Upon desolvation, the colloids coalesce to form a Rigid Amorphous Metal Rich (RAMETRIC) phase. The coalescence of colloids to form the RAMETRIC phase is similar to a sol-gel transition.

The RAMETRIC phase is similar to both a gel-phase and a glass-phase but fits the technical definitions for neither. Compared to gels, the transition from sol to gel occurs at very low hydration (5% solvent) and creates a rigid (not gel-like) and nearly amorphous material. In contrast, gels typically have a very high-water content (≥98% by mass). Like glasses, the RAMETRIC phase is amorphous and rigid. However, glasses are characterized by defined temperature-based phase transitions (e.g., from molten to glass or molten to crystalline). The RAMETRIC phase has no such temperature-based transitions; rather it is a near-amorphous solid at lower temperatures and decomposes at higher temperatures.

The RAMETRIC phase has unprecedented hydration-state dependent rigidity, as determined by rheological measurement. The material's atypical rheological properties arise from a fundamentally different nanoscale structure than observed for previously described Ag-cys hydrogels. The emergent rigidity is attributed to the formation of a continuous network in the gel-phase. Whereas Ag-cys hydrogels formed without diglyme are comprised of stacked sheets (like graphite), the RAMETRIC material comprises a continuous network (like diamond).

Hierarchical structures assemble in discrete stages, starting with molecular-level interactions that form structures that then assemble in a higher order into superstructures, and so on. We found that by disrupting the self-assembly process that typically forms a network of networks, our identical constituents instead assemble into a continuous network, where molecular-level interactions span the entire volume of the material. The disruption of a hierarchical self-assembly process to form a single continuous network is unprecedented in the literature. The resulting material engenders an entirely different ensemble of properties unachievable through incremental advancements. Further exploration of this process may translate to supramolecular gels of all compositions, opening the door to many new structure-property relationships and soft-materials applications.

RESULTS AND DISCUSSION

Synthesis of sol-RAMETRIC material

The mixture of Ag(I) and cysteine in the presence of diglyme results in a phase-separated product. The majority of Ag(I) and cysteine is found in a dense sol phase. The upper (solvent) phase, presumably containing any unreacted Ag(I), cysteine, and counterions is discarded. A full description of the synthesis may be found in the supporting information.

The dense-sol phase thickens as it dries and exhibits rheological properties dependent on moisture content. Sufficient dehydration triggers a sol-RAMETRIC transition, analogous to a sol-gel transition. The sol-RAMETRIC transition is reversible; rehydration returns the RAMETRIC phase to the sol phase. The sol-RAMETRIC transition is completely reversible by simple dehydration / rehydration.

Study of the sol-RAMETRIC system at various moisture contents revealed the role of water in the sol-RAMETRIC transition. Equilibration in relative humidity (RH) chambers containing saturated salt solutions provided consistent control over moisture content due to the hygroscopic nature of the material. Supplementary Table 1 lists the relative humidities obtained for 6 different saturated salt solutions at equilibrium. The sol-RAMETRIC transition was studied at each of these 6 relative humidity values. Oscillatory strain rheology performed on these samples pinpoints the moisture content that defines the gel point during the sol-gel transition (Figure 1).

Measuring the elastic (G') and viscous (G") moduli for each sample reveals the moisture content for the RAMETRIC (solid) phase (G'>G") and colloidal sol-phase (G">G'). Measurements were averaged across low strains to ensure the recorded moduli accurately represent an intact network. Figure 1a plots moduli for each sample as a function of moisture content. The data for samples at and below 4.9% moisture are RAMETRIC phase, while samples at and above 7.9% moisture content are colloidal sol-phase. This data therefore indicates a sol-RAMETRIC transition between 4.9% and 7.4% moisture content.

The data confirm the sol thickens as it dries by displaying an initial increase in moduli. Remarkably, this trend does not continue beyond the sol-RAMETRIC phase transition. Once the RAMETRIC phase forms, further dehydration results in a moduli decrease, representing a weakening and degradation of the material. Thus, the data suggests a moisture content near the sol-RAMETRIC transition where the gel is in its most rigid state. This observation posits water in a structural role in the sol-

RAMETRIC transition, where dehydration past the transition point removes structural water, weakening the network. Consistent with a structural role for water, complete desiccation disintegrates the RAMETRIC into a powder.

The material is solid under *ca.* 5% moisture content and exhibits G' ~ 10^7 Pa. Typical G' for coinage-metal thiolate hydrogels with similar composition are on the order of 10^1 Pa, while attempts to increase G' through incorporation into elastomeric networks plateaued at 10^3 Pa.[18] Conversion of G' to Young's modulus (E'), a measure of uniaxial elastic deformation commonly reported for engineering materials (Supplementary Equation 1), allows a comparison of RAMETRIC rigidity to that of other materials. Figure 1b illustrates this range in a property chart of E' vs. density with comparison to common engineering materials.[19] The RAMETRIC phase exhibits a modulus comparable to polymers and elastomers. The increase in moduli over metallophilic hydrogels of nearly identical composition is clearly more than incremental. Such an advancement potentially renders the RAMETRIC phase as an engineering-grade material on par with carbon-based polymers. Here, the high metal ion content is especially unusual for materials with this combination of density and rigidity.

Figure 1c depicts viscosity measurements of the sol phase over a broad range of moisture contents, providing insight into the structural nature of the material when compared to polymeric materials. Viscosity as a function of moisture is well-fit by the equation $y = 5 \times 10^{-12}x^{-8.08}$ (Figure 1c). Whereas organic polymers at various degrees of solvation exhibit entangled non-linear viscoelastic, semi-dilute, and dilute linear viscous Newtonian regimes, the continuous change in viscosity as a function of solvation for the sol posits water as a classical solvent. This difference indicates the colloidal phase does not interact with solvent like polymeric materials do. This is interpreted as that the metallopolymers comprising the sol are not polymeric but oligomeric. Overall, the rheological response of the sol-phase resembles a colloidal system more than a polymeric one.

X-Ray diffraction (XRD) and Scanning Electron Microscopy (SEM) measurements of the RAMETRIC phase elucidate aspects of the structure that underlie the unusual rheological properties. Both measurements show the material as nearly-amorphous at the highest level of structural description. SEM imaging of the RAMETRIC phase (Figure 2a) shows a continuous, featureless landscape. The lack of any observable microstructure suggests the material as amorphous. Similarly, the XRD analysis shows almost no ordering. A broad peak at 6° 2θ (1.47 nm) indicates some long-range order (Figure 2b). The presence of only one XRD feature, its diffuse nature, and the small angle of scattering suggest that crystalline regularity is essentially absent in the RAMETRIC phase. All other observed peaks are attributable to the polypropylene (PP) film that supported the RAMETRIC material during the measurement.

The XRD measurement shows that the material does not contain Ag^0 nanocrystals, which generate a diffraction pattern characteristic of Ag^0.[20] XRD measurements of a silver-cysteine material made in without diglyme, but in otherwise identical conditions shows 7 sharp peaks at 2θ values between 5 and 40°, suggesting a highly crystalline material (Figure S1). Likewise, SEM of the material formed in the absence of diglyme shows faceted crystalline materials (Figure S1).

Electron microscopy (EM) provides additional structural insight into this amorphous material. SEM of the RAMETRIC-phase shows smooth, flat surfaces with cracks that formed as the gel dried (Figure 2a). There is no evidence of sub-surface structure within these cracks (Figure 2a, inset), implying the amorphous material is also uniform. In contrast, in CMTP hydrogel systems, the 2D metallopolymer sheets stack to form 3D fibrils with distinctive structure observable through SEM.[11] The lack of structural similarity between these two gel-phase materials of nearly identical composition is striking and indicates a fundamental change in molecular structure. Cryogenic high-angle annular dark field (HAADF) scanning transmission electron microscopy (STEM) was used to acquire images of the sol-phase. Figure 2c shows the colloids present in the sol at 95% water by weight. At this hydration, the nanoparticles are approximately 50 nm in diameter. Notably, the edges of the colloids are indistinct, implying that the colloids have poorly defined boundaries. Figure 2d shows a higher magnification image of the same sample. In this image, there is evidence for coalescence of individual colloids into the RAMETRIC phase. In Figure 2, the combination of images that show colloidal material in the sol phase (panel 2c), partial coalescence in the sol phase, and total coalescence in the RAMETRIC phase (panel 2A), constitute evidence for coalescence of individual colloids into the continuous RAMETRIC phase.

Gel permeation chromatography with multi-angle light scattering (GPC-MALS) also supports a colloidal sol-phase. GPC-MALS (Figure S2) measurement shows a hydrodynamic radius (R_H) of colloids to be 41.4±0.3% nm and the radius of gyration (R_G) to be 277±0.3% nm. Dynamic light scattering (DLS) corroborates the ca. 40 nm colloidal phase (Figure S6). Since R_H defines the radius of a hard sphere and R_G defines that of a mass-weighted average, the ratio between the two values provides insight into colloid structure. Observation of R_G/R_H ~ 6.7 in this system suggests the colloids are loosely packed, non-spherical agglomerates. This is consistent with the cryo-EM observation. For comparison, globular proteins or tightly bound polymer coils characteristically exhibit $R_G/R_H \leq 1$.

Colloid Composition

The colloids of the sol-phase are comprised of cysteine, silver, and sodium. Inductively coupled plasma mass-spectroscopy (ICP-MS) analysis of the sol suggests molar ratios of 5:2:2 Ag:S:Na. A 2.5-fold excess of Ag over cysteine is unexpected and is unique among Ag-cys metallopolymer reports where CMTPs are well-known to exist in 1:1 M:SR stoichiometry.[11]

Carbon-13 nuclear magnetic resonance (^{13}C NMR) suggests that all three of cysteine's functional groups are bound to Ag^+ or Na^+ in some way (Figure S3, Table S2). Density functional theory (DFT) simulations of binding energies among colloidal component molecules were used to interpret the stoichiometric ratios of Ag and Na to cysteine in the context of promiscuous binding observed in ^{13}C NMR results. Bond dissociation energies (BDEs) were calculated for both Ag^+ and Na^+ cations with the thiol, carboxylic, and amine groups of cysteine, as well as for possible cysteine dimer configurations coordinated through these cations. The BDEs of the most stable conformers for Ag^+ and Na^+ coordination are given in Supplementary Table 3 and depicted graphically in Figure 3. Ag^+ binding energies to cysteine functional groups are always larger than those for Na^+ and generally follow $S>NH_2>COO^-$.

Of cysteine's three functional groups, Ag^+ binds least strongly to COO^-, while Na^+ binds most strongly to this group. Sodium present in the sol and RAMETRIC phases is therefore expected to coordinate with COO^- groups. The weaker nature of the Na-cysteine interactions compared to Ag-cysteine also suggests that these Na-cysteine bonds will be more readily broken up by water with increasing moisture content, while Ag-cysteine bonds resist dissolution. BDE calculations collectively predict a molecular structure within the sol-phase that consists of short-chain -Ag-S- oligomers crosslinked through side-chain bonds to Ag^+; all Na^+ in the system is expected to coordinate to COO^-, shown in Figure 3. Further discussion on DFT calculations is available in Note S1.

Solid state ^{13}C NMR of pure cysteine displays three sharp peaks that correspond to the nearest carbon for each functional group of cysteine: CH_2-S, CH-NH_2, and COO (Figure S3). In comparison, the RAMETRIC phase displays very broad peaks shifted upfield from pure cysteine for the CH_2-S and CH-NH_2 functional groups. The peak corresponding to COO is also broadened and shifted upfield, but not to the same extent as the CH_2-S and CH-NH_2 peaks. This suggests that some COO groups are not coordinated by cations (Figure S3). The breadth of all the RAMETRIC phase peaks indicates that binding around cysteine is highly disordered and exists in a variety of conformations. ^{1}H-NMR, 2D ^{1}H{^{13}C} HSQC, and ^{1}H COSY are supplied in Supplementary Figures 7 and 8.

Sol-RAMETRIC Transition

A structural model of the sol-RAMETRIC transition for these colloids is informed by Fourier transform infrared spectroscopy (FTIR) and ^{23}Na NMR analysis of material in both the sol and the RAMETRIC state. FTIR shows a distinct change for the cysteine COO^- group in the hydrated (sol) versus dehydrated (RAMETRIC) states. Relative to free cysteine, the sol-state cysteine COO^- and NH_2 groups shift to lower energies (7 and 4 cm^{-1}, respectively, Figure 4). This implicates cation (Na^+ or Ag^+) binding to both carboxylate and amine groups of cysteine in sol.

The COO^- peak for the RAMETRIC phase shows a larger redshift of 24 cm^{-1}. A shift of this magnitude is characteristic of cation coordination. Thus, available cations (Ag^+ or Na^+) become coordinated to the COO^- group during the transition from sol to RAMETRIC. The reversible nature of the sol-RAMETRIC transition implies that cation coordination is broken by solvation. BDE calculations (*vide supra*) point to COO^- as the most likely site for Na^+ coordination, and the relatively weak binding energies for COO-Na imply that dissolution of these bonds occurs more readily than cysteine-Ag bonds. Taken together, this body of FTIR and computational data suggests that Na^+ coordination to COO^- facilitates the sol-RAMETRIC transition.

^{23}Na NMR experiments support Na^+ coordination to COO^- during the sol-RAMETRIC transition. A dilute solution of the sol exhibits a sharp peak at 0.2 ppm for Na^+ referenced to a 10 mM NaCl solution (Figure S5). This suggests that Na^+ is essentially aqueous in the sol phase. This data also suggests Na^+ is excluded from the colloidal component, as colloidally contained Na^+ would produce a second ^{23}Na NMR peak. Indeed, diffusion ordered spectroscopy (DOSY) ^{23}Na NMR gives similar diffusion coefficients for Na^+ in both the sol and in aqueous form (Table S8). In contrast to the single, sharp peak for ^{23}Na in the sol state, solid-state ^{23}Na NMR of the RAMETRIC phase shows a single, very broad peak with a chemical shift at -22.1 ppm (Figure S5). The breadth of the RAMETRIC-phase peak is consistent with multiple bonding conformations that arise in the sol-RAMETRIC transition.

Overall, this data suggests that Na^+ facilitates the sol-RAMETRIC phase-change. In the sol-phase, Na^+ is fully solvated by water; in the RAMETRIC phase, it coordinates any free COO^- groups, facilitating bridging interactions among coalescing colloids. Similar behavior is observed in Na-montmorillonite clays, which exhibit peak shift and broadening in their NMR spectra as the clays dry and trap Na^+ within the interlayer spaces of microstructures.[21]

FTIR of the sol and RAMETRIC phase shows an insignificant peak shift for NH_2, implying no coordination change during the sol-RAMETRIC transition. This NH_2 peak broadens significantly in the RAMETRIC phase compared to the sol, suggesting a more disordered NH_2 coordination environment is brought about by desiccation. Considering the excess of Ag^+ observed in ICP-MS, and the DFT-predicted Ag-N bonding favorability (Figure 3), the cysteine NH_2 is forming dative bonds to Ag^+. Since these bonds crosslink the -Ag-S- oligomers within the colloids, water must exist within the colloids and must be drawn out to some extent during dehydration. The interparticle network thus rearranges through water loss and disturbs the hydrogen bond network around the NH_2 moiety, producing a broad peak observed through FTIR.

An Integrative Model for the sol-RAMETRIC material

This chaotic assembly of loosely bound metal complexes into the RAMETRIC phase results in a rigidity distinctly greater than any previously reported material created from the same components. To explain this, a model shown in Figure 5 helps explain the rigidity observed by rheological measurement. This model integrates all of the data presented above into a self-consistent model of RAMETRIC phase formation.

At the atomic structure level, metal-thiolate oligomers (Figure 5a) comprise the colloids (Figure 5b, c). The model presented in Figure 5a and 5b is consistent with the NMR, DFT, and ICP-MS data. Dehydration of the colloidal phase provokes the sol-RAMETRIC transition (Figure 5c, d), as supported by rheology data. The RAMETRIC phase is strengthened by ion bridging between carboxylic acids of adjacent colloids (Figure 5e, f) which becomes favorable at low water content. These bridging interactions are supported by solid-state NMR and FTIR measurements.

The presence of excess water within the sol-phase colloids imparts generous flexibility to the colloid, consistent with cryo-EM and GPC data. The flexible colloids can adopt arbitrary morphology during sol-gel transition, as observed by cryo-EM. In this scenario, dehydration drives colloid assembly in the sol-RAMETRIC transition, minimizing void spaces and maximizing surface interactions. This critical moisture content defines the sol-RAMETRIC transition, where only structural water molecules remain. Rheology results reflect that dehydration past this point removes structural water, resulting in weaker material.

At the sol-RAMETRIC transition point, the material can be considered as a densely packed network of flexible colloids. Because the colloids adopt whatever shape is needed to maximize colloid-to-colloid interactions (Figure 5e), the RAMETRIC phase appears as a continuous network. This continuous network model (of Figure 5) is supported directly by SEM imaging and X-Ray Diffraction; the continuous network model is indirectly supported by rheometric (mechanical) measurement and by Na^+ binding calculations (where Na^+ plays the role of bridging colloids in the RAMETRIC phase). Other structural models that we consider for the material cannot integrate these data.

In contrast to the continuous network postulated here, CMTP hydrogels—the material that forms from Ag-cys building blocks in the absence of glyme—are hierarchical structures comprised of stacked sheets. The relative weakness of these materials arises from susceptibility of the stacked-sheets to slippage under shear forces. The continuous network formed in the RAMETRIC phase is not susceptible to such shear-forces; conceptually this is like elemental carbon in graphite (CMTP gels) vs diamond (RAMTERIC phase).

While the studies reported herein utilized silver as a case study to elucidate RAMETRIC structure, these materials are not limited to silver-based systems. Our group reported the first instance of a RAMETRIC phase in 2016 with copper[22] and has since synthesized sol-RAMETRIC phases with gold, nickel, and tin (Figure S9). Independent of metal cation choice, all sol-RAMETRIC materials exhibit the same properties: a rigid RAMETRIC phase, a reversible sol-RAMETRIC transition, and a sol phase comprised of amorphous colloids. While preliminary, these results suggest the broad applicability of glyme-disrupted self-assembly may be applicable to other metallosupramolecular materials.

A synthetic approach that generates silver-cysteine Sol-RAMETRIC materials with surprising emergent solid-phase rigidity is reported. Inclusion of an anti-solvent during synthesis precipitates the precursors as a colloidal sol which forms a RAMETRIC phase upon dehydration. Structural water and cation coordination is necessary to stabilize the molecular network of the RAMETRIC phase. Simulation and experimentation in concert suggest the RAMETRIC phase is a continuous network, akin to a carbon-based polymer. This work opens the door to rational design of RAMETRIC phases with previously inaccessible rigidity, representing a new metal-rich soft material.

A continuous metal-ligand network resolves the origin of the rigidity observed for the RAMETRIC phase. Sol-RAMETRIC materials disrupt a previously hierarchical self-assembly process, forming instead a continuous molecular network reminiscent of glasses and polymers. Indeed, the exceptional increase in Young's modulus is on the order of silicon- and carbon-based

polymeric materials. While generally assumed to be weak interactions, the metal-ligand bonds underpinning the RAMETRIC phase exhibit a strength in numbers that result in a new class of rigid metal-ion based materials.

EXPERIMENTAL PROCEDURES

Full experimental procedures are provided in the Supplemental Information Document.

Resource Availability

Lead Contact

Further information and requests for resources and reagents should be directed to and will be fulfilled by the Lead Contact, Christopher J. Ackerson (ackerson@colostate.edu).

Materials Availability

Samples of the sol-RAMETRIC material are available upon request. For synthesis, all Materials were purchased through Sigma-Aldrich. 1,2-dimethyoxyethane (anhydrous, 99.5%, inhibitor-free), DL-cysteine (technical grade), silver nitrate (ACS reagent, ≥99.0%), sodium hydroxide (certified ACS pellets). Water used was nanopure water. Salts used for relative humidity chambers were potassium carbonate (anhydrous, ACS reagent ≥99%), potassium acetate (ACS grade), lithium chloride (ACS reagent, ≥99%), lithium bromide (ReagentPlus®, ≥99%), magnesium chloride (anhydrous, ≥98%), magnesium nitrate hexahydrate (ACS reagent, ≥99%).

Data and Code Availability

This study did not generate/analyze datasets.

SUPPLEMENTAL INFORMATION

Supplemental Information Document. Supplemental experimental procedures, Equation SE1, Tables ST1- ST4, Figures S1-S9, and Note S1

ACKNOWLEDGMENTS

The authors thank Nick Colella for his contributions to discussions of microstructure analysis.
CJA and JA acknowledge support from NSF 1507646
The authors acknowledge funding from Lawrence Livermore National Laboratory (Grant no. 18-LW-063).
Work at the Molecular Foundry was supported by the Office of Science, Office of Basic Energy Sciences, of the U.S. Department of Energy under Contract No. DE-AC02-05CH11231.

AUTHOR CONTRIBUTIONS

J.A., P.S., W.S.C. conceived the idea. J.A., C.C. synthesized material. J.A., T.B., W.S.C., and J.L. performed and interpreted rheological measurements. J.A., H.M. collected and interpreted NMR data. J.A., K.M. collected and interpreted XRD and DLS measurements. M.T. analyzed experimental data to elucidate structure-property relationships. J.L. analyzed and interpreted GPC-MALS data. P.S. and B.W. conceived, modeled, performed, and interpreted computational methods and data. B.F.G. collected cryo-electron microscopy data and interpreted data alongside C.J.A and W.S.C. J.A., C.J.A., and W.S.C. discussed results to elucidate the schematic representation. The manuscript was written and revised by J.A., P.S., B.W., B.F.G., C.J.A., and W.S.C. All authors approve the final version of the manuscript.

DECLARATION OF INTERESTS

The authors declare the following competing interests:
The authors M.A.T, C.J.A., and W.S.C own shares in AEMS Corp.

Figure 1: Physical properties of the sol-RAMETRIC material.

a) Comparison of G' (blue square) and G" (green circle) for different moisture contents around the sol-RAMETRIC transition. b) Ashby chart of Young's modulus vs. density of RAMETRIC phase compared to engineering materials. c) Viscosity of sol at varying moisture contents greater than the sol-RAMETRIC transition.

Figure 2: Structural investigation of sol and RAMETRIC phases.

a) SEM micrograph of dehydrated RAMETRIC phase showing lack of microstructure in material. Zoom inset of crack formed during dehydration shows sub-surface structure is uniform; scale bars are 10 μm and 1 μm for the SEM micrograph and Zoom inset images respectively. b) XRD of RAMETRIC powder (orange dash trace) and the polypropylene film substrate (blue solid trace). c) cryo-HAADF STEM image of ~5% Ag-cys sol-phase in vitreous ice showing colloidal densities (lighter areas) on the order of 50 nm, scale bar is 500 nm. d) cryo-HAADF STEM image of ~5% Ag-cys sol-phase in vitreous ice at higher magnification emphasizing the coalescence of amorphous colloidal densities (light areas), scale bar is 100 nm.

Figure 3: DFT calculations of bond dissociation energies (BDE).

a) Cartoon legend of cysteine and 1,2-dimethoxyethane (DME) with Ag^+ and Na^+ ions shown in possible bonding configurations. b,c) Radar graphs depicting BDE (eV) of Na^+ and Ag^+ bound to functional groups of cysteine and DME for b) singly bound configurations and c) additional doubly bound configurations. d,e) Radar graphs depicting BDE (eV) of all bonds simulated in solvent and in vacuum for cysteine and DME bonds to d) Na^+ and e) Ag^+.

Figure 4: FTIR of sol-RAMETRIC assemblies and their components.

Solid phase cysteine is shown as a solid blue trace, dehydrated RAMETRIC as a dashed orange trace, and hydrated RAMETRIC as a dot-dashed green trace. Absorbance values are scaled so peak heights are equivalent to highlight comparisons between a) C=O and b) NH_2 stretches.

Figure 5: Scheme of RAMETRIC structure and method of agglomeration.

a) Molecular structure of linear silver-cysteine oligomers (purple) bridged through cysteine side chains by free Ag^+ ions (green). b) Illustration of silver-thiolate oligomers (purple lines) bridged by Ag^+ (green lines). c) colloidal sol containing flexible, globular colloids solvated by water with aqueous Na^+ ions. d) Dehydration drives the reversible sol-RAMETRIC transition as colloids agglomerate and trap Na^+ ions. The flexible colloids are expected to alter their shape to minimize void space. e,f) Insets of interstitial space between colloids in the e) RAMETRIC state, where Na^+ binds to cysteine's carboxylic acid functional groups, and f) sol state, where aqueous Na^+ ions are freely soluble.

References

1. Fages, F. Metal Coordination To Assist Molecular Gelation. Angew. Chem. Int. Ed. 2006, 45 (11), 1680–1682. https://doi.org/10.1002/anie.200503704.
2. Piepenbrock, M.-O. M.; Lloyd, G. O.; Clarke, N.; Steed, J. W. Metal- and Anion-Binding Supramolecular Gels. Chem Rev 2010, 110 (4), 1960–2004. https://doi.org/10.1021/cr9003067.
3. Söptei, B.; Mihály, J.; Szigyártó, I. Cs.; Wacha, A.; Németh, C.; Bertóti, I.; May, Z.; Baranyai, P.; Sajó, I. E.; Bóta, A. The Supramolecular Chemistry of Gold and L-Cysteine: Formation of Photoluminescent, Orange-Emitting Assemblies with Multilayer Structure. Colloids Surfaces Physicochem Eng Aspects 2015, 470, 8–14. https://doi.org/10.1016/j.colsurfa.2015.01.048.
4. Chen, L.-J.; Yang, H.-B. Construction of Stimuli-Responsive Functional Materials via Hierarchical Self-Assembly Involving Coordination Interactions. Accounts Chem Res 2018, 51 (11), 2699–2710. https://doi.org/10.1021/acs.accounts.8b00317.
5. Liu, M.; Ouyang, G.; Niu, D.; Sang, Y. Supramolecular Gelatons: Towards the Design of Molecular Gels. Org Chem Front 2018, 5 (19), 2885–2900. https://doi.org/10.1039/c8qo00620b.
6. Cook, T. R.; Zheng, Y.-R.; Stang, P. J. Metal–Organic Frameworks and Self-Assembled Supramolecular Coordination Complexes: Comparing and Contrasting the Design, Synthesis, and Functionality of Metal–Organic Materials. Chem Rev 2013, 113 (1), 734–777. https://doi.org/10.1021/cr3002824.
7. Zhu, Q.-L.; Xu, Q. Metal-Organic Framework Composites. Chem Soc Rev 2014, 43 (16), 5468–5512. https://doi.org/10.1039/c3cs60472a.
8. Fucke, K.; Peach, M. J. G.; Howard, J. A. K.; Steed, J. W. A New WaterNa + Coordination Motif in an Unexpected Diatrizoic Acid Disodium Salt Crystal Form. Chem Commun 2012, 48 (79), 9822–9824. https://doi.org/10.1039/c2cc32766j.
9. Kumar, D. K.; Steed, J. W. Supramolecular Gel Phase Crystallization: Orthogonal Self-Assembly under Non-Equilibrium Conditions. Chem Soc Rev 2014, 43 (7), 2080–2088. https://doi.org/10.1039/c3cs60224a.
10. Randazzo, R.; Mauro, A. D.; D'Urso, A.; Messina, G. C.; Compagnini, G.; Villari, V.; Micali, N.; Purrello, R.; Fragalà, M. E. Hierarchical Effect behind the Supramolecular Chirality of Silver(I)–Cysteine Coordination Polymers. J Phys Chem B 2015, 119 (14), 4898–4904. https://doi.org/10.1021/acs.jpcb.5b00847.
11. Odriozola, I.; Ormategui, N.; Loinaz, I.; Pomposo, J. A.; Grande, H. J. Coinage Metal–Glutathione Thiolates as a New Class of Supramolecular Hydrogelators. Macromol Symp 2008, 266 (1), 96–100. https://doi.org/10.1002/masy.200850618.

12. Odriozola, I.; Loinaz, I.; Pomposo, J. A.; Grande, H. J. Gold–Glutathione Supramolecular Hydrogels. J Mater Chem 2007, 17 (46), 4843–4845. https://doi.org/10.1039/b713542d.
13. Veselska, O.; Demessence, A. D10 Coinage Metal Organic Chalcogenolates: From Oligomers to Coordination Polymers. Coordin Chem Rev 2018, 355, 240–270. https://doi.org/10.1016/j.ccr.2017.08.014.
14. Veselska, O.; Guillou, N.; Diaz-Lopez, M.; Bordet, P.; Ledoux, G.; Lebègue, S.; Mesbah, A.; Fateeva, A.; Demessence, A. Sustainable and Efficient Low-Energy Light Emitters: A Series of One-Dimensional d 10 Coinage Metal–Organic Chalcogenolates, [M(o -SPhCO 2 H)] n. Chemphotochem 2022, 6 (5). https://doi.org/10.1002/cptc.202200030.
15. Leung, B. O.; Jalilehvand, F.; Mah, V.; Parvez, M.; Wu, Q. Silver(I) Complex Formation with Cysteine, Penicillamine, and Glutathione. Inorg Chem 2013, 52 (8), 4593–4602. https://doi.org/10.1021/ic400192c.
16. Datta, S.; Saha, M. L.; Stang, P. J. Hierarchical Assemblies of Supramolecular Coordination Complexes. Accounts Chem Res 2018, 51 (9), 2047–2063. https://doi.org/10.1021/acs.accounts.8b00233.
17. Boonkaew, B.; Kempf, M.; Kimble, R.; Supaphol, P.; Cuttle, L. Antimicrobial Efficacy of a Novel Silver Hydrogel Dressing Compared to Two Common Silver Burn Wound Dressings: ActicoatTM and PolyMem Silver®. Burns 2014, 40 (1), 89–96. https://doi.org/10.1016/j.burns.2013.05.011.
18. Luzuriaga, A. R. de; Rekondo, A.; Martin, R.; Cabañero, G.; Grande, H. J.; Odriozola, I. “Metallophilic Crosslinking” to Provide Fast-curing and Mendable Poly(Urethane-metallothiolate) Elastomers. J. Polym. Sci. A Polym. Chem. 2015, 53 (9), 1061–1066. https://doi.org/10.1002/pola.27534.
19. ASHBY, M. F.; CEBON, D. Materials Selection in Mechanical Design. Le J De Physique Iv 1993, 03 (C7), C7-1-C7-9. https://doi.org/10.1051/jp4:1993701.
20. Chang, Y.-M.; Lu, I.-T.; Chen, C.-Y.; Hsieh, Y.-C.; Wu, P.-W. High-Yield Water-Based Synthesis of Truncated Silver Nanocubes. J Alloy Compd 2014, 586, 507–511. https://doi.org/10.1016/j.jallcom.2013.10.047.
21. Ohkubo, T.; Saito, K.; Kanehashi, K.; Ikeda, Y. A Study on Hydration Behaviors of Interlayer Cations in Montmorillonite by Solid State NMR. Sci Technol Adv Mat 2004, 5 (5–6), 693–696. https://doi.org/10.1016/j.stam.2004.02.016.
22. Compel, W. S. Metallogels through Glyme Coordination. Dalton Transactions Camb Engl 2003 2016, 45 (11), 4509–4512. https://doi.org/10.1039/c6dt00255b.

Cell Reports
Physical Science

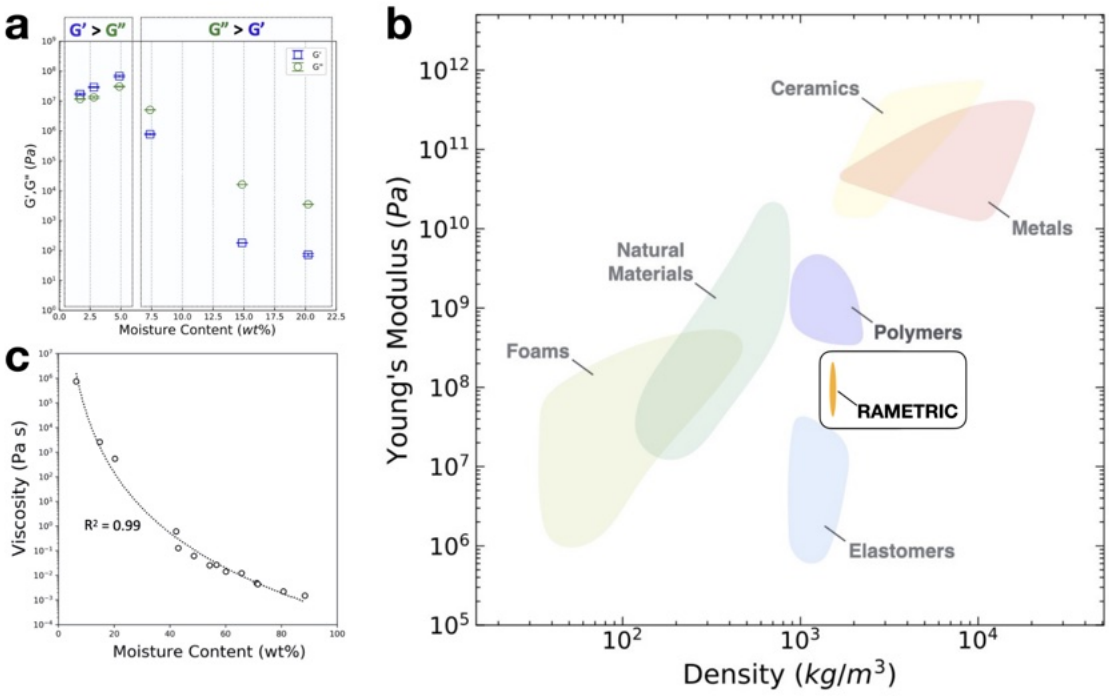

Figure 1: Physical properties of sol-RAMETRIC material.

a) Comparison of G' (blue square) and G" (green circle) for different moisture contents around the sol-RAMETRIC transition. b) Ashby chart of Young's modulus vs. density of the RAMETRIC phase compared to engineering materials. c) Viscosity of sol at varying moisture contents greater than the sol-RAMETRIC transition.

Cell Reports
Physical Science

CellPress

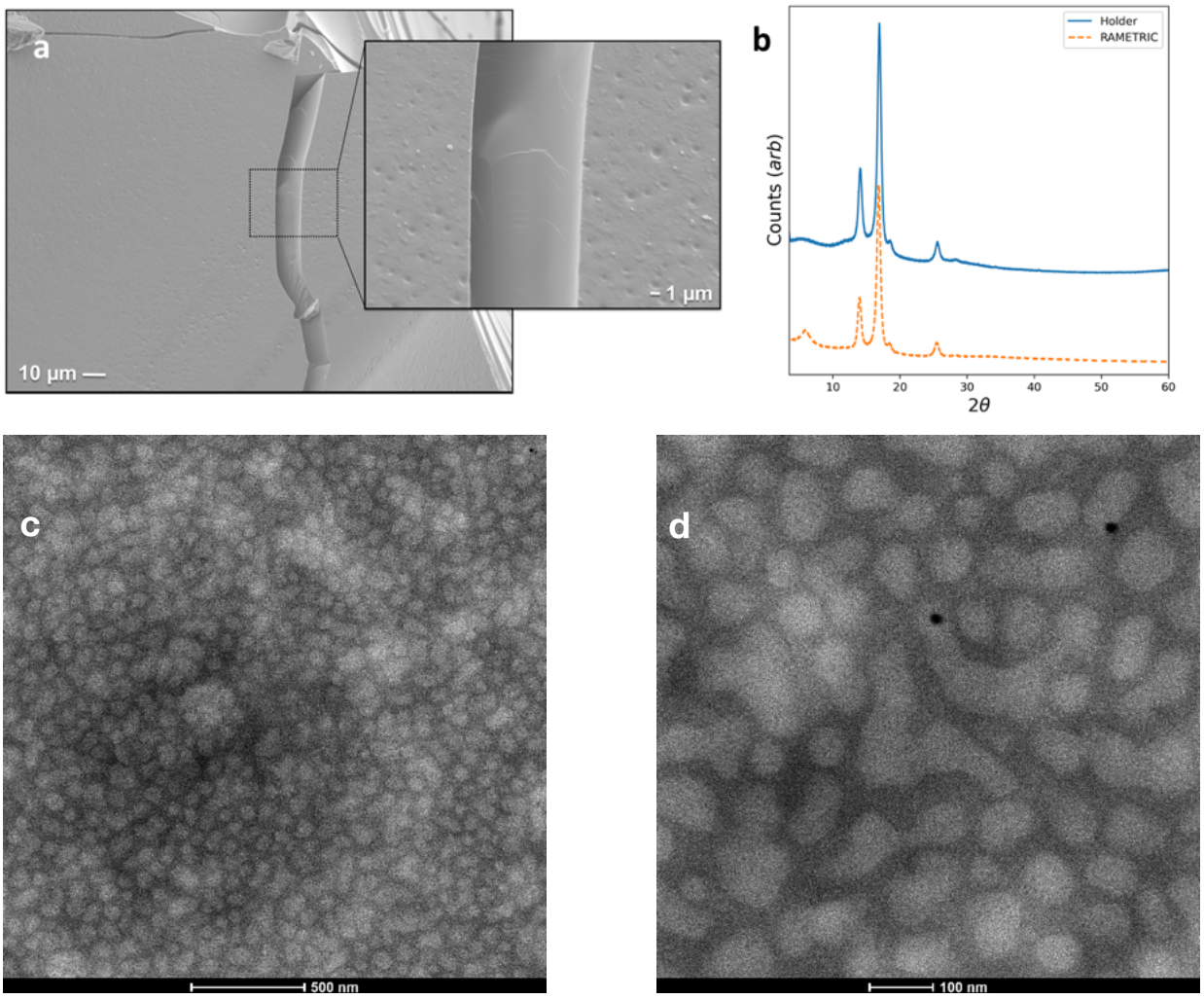

Figure 2: Structural investigation of sol and RAMETRIC phases.

a) SEM micrograph of dehydrated RAMETRIC phase showing lack of microstructure in material. Zoom inset of crack formed during dehydration shows sub-surface structure is uniform; scale bars are 10 µm and 1 µm for the SEM micrograph and Zoom inset images respectively. b) XRD of RAMETRIC powder (orange dash trace) and the polypropylene film substrate (blue solid trace). c) cryo-HAADF STEM image of ~5% Ag-cys sol-phase in vitreous ice showing colloidal densities (lighter areas) on the order of 50 nm, scale bar is 500 nm. d) cryo-HAADF STEM image of ~5% Ag-cys sol-phase in vitreous ice at higher magnification emphasizing the coalescence of amorphous colloidal densities (light areas), scale bar is 100 nm.

Cell Reports
Physical Science

CellPress

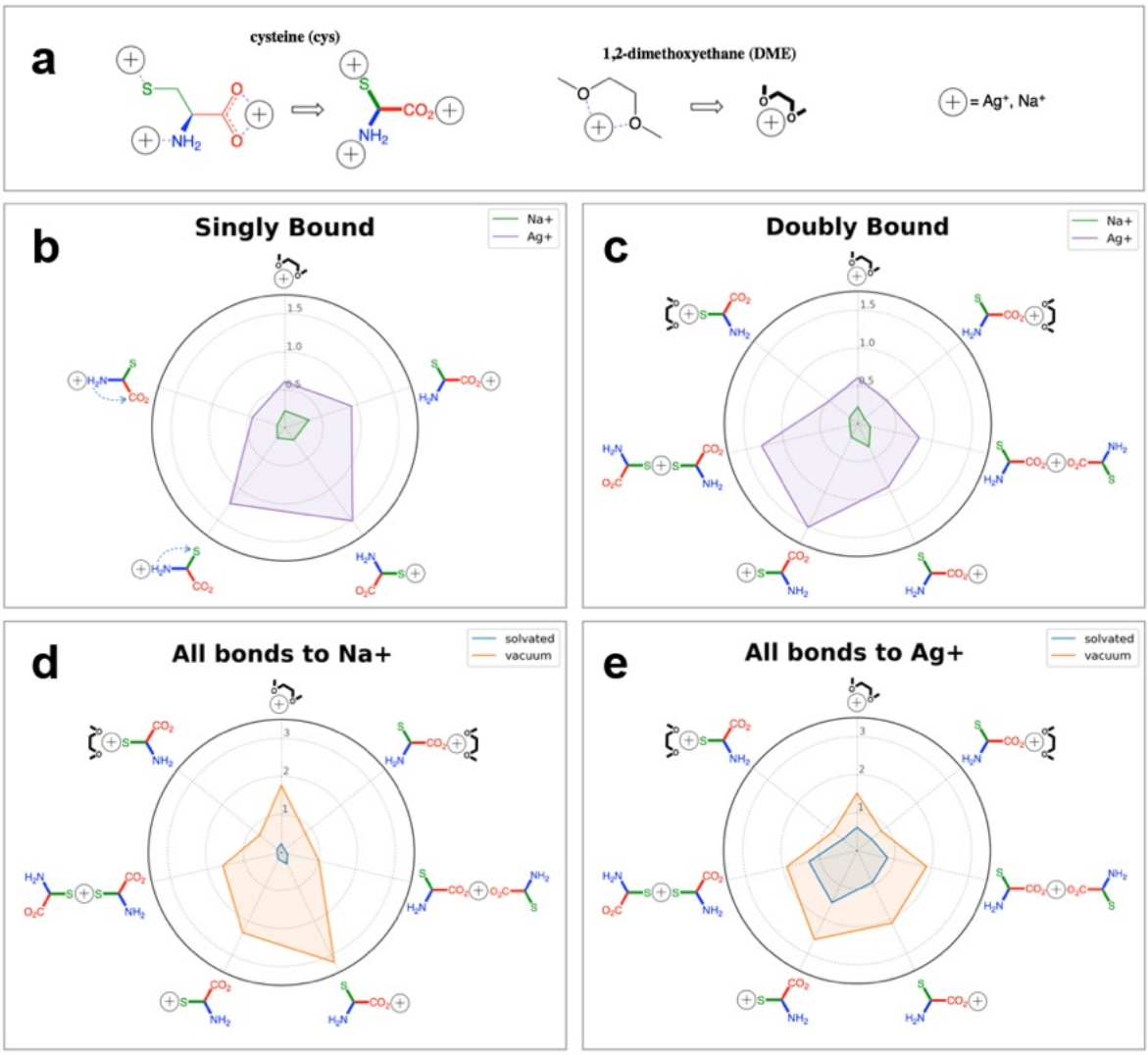

Figure 3: DFT calculations of bond dissociation energies (BDE).

a) Cartoon legend of cysteine and 1,2-dimethoxyethane (DME) with Ag^+ and Na^+ ions shown in possible bonding configurations. b,c) Radar graphs depicting BDE (eV) of Na^+ and Ag^+ bound to functional groups of cysteine and DME for b) singly bound configurations and c) additional doubly bound configurations. d,e) Radar graphs depicting BDE (eV) of all bonds simulated in solvent and in vacuum for cysteine and DME bonds to d) Na^+ and e) Ag^+.

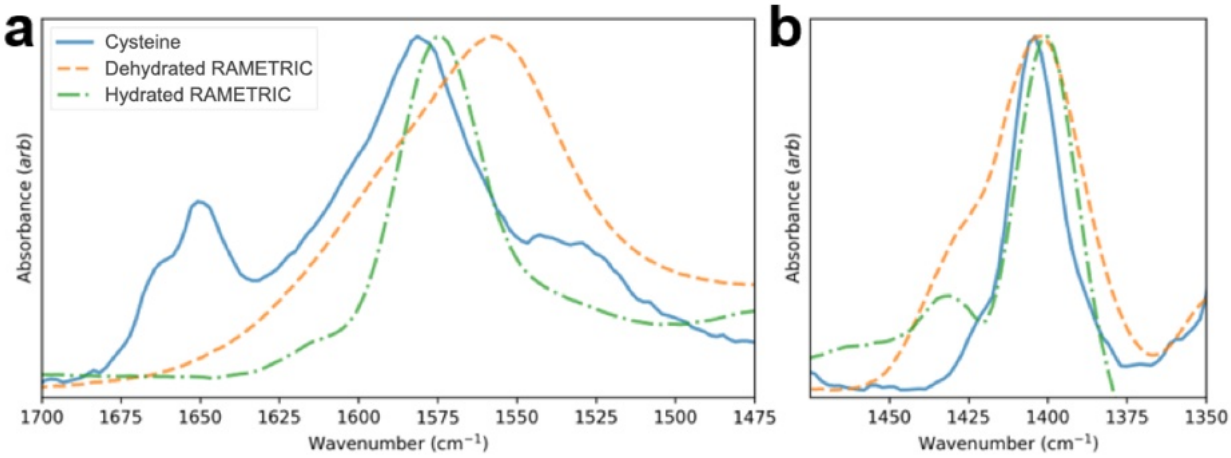

Figure 4: FTIR of sol-RAMETRIC assemblies and their components.

Solid phase cysteine is shown as a solid blue trace, dehydrated RAMETRIC as a dashed orange trace, and hydrated RAMETRIC as a dot-dashed green trace. Absorbance values are scaled so peak heights are equivalent to highlight comparisons between a) C=O and b) NH_2 stretches.

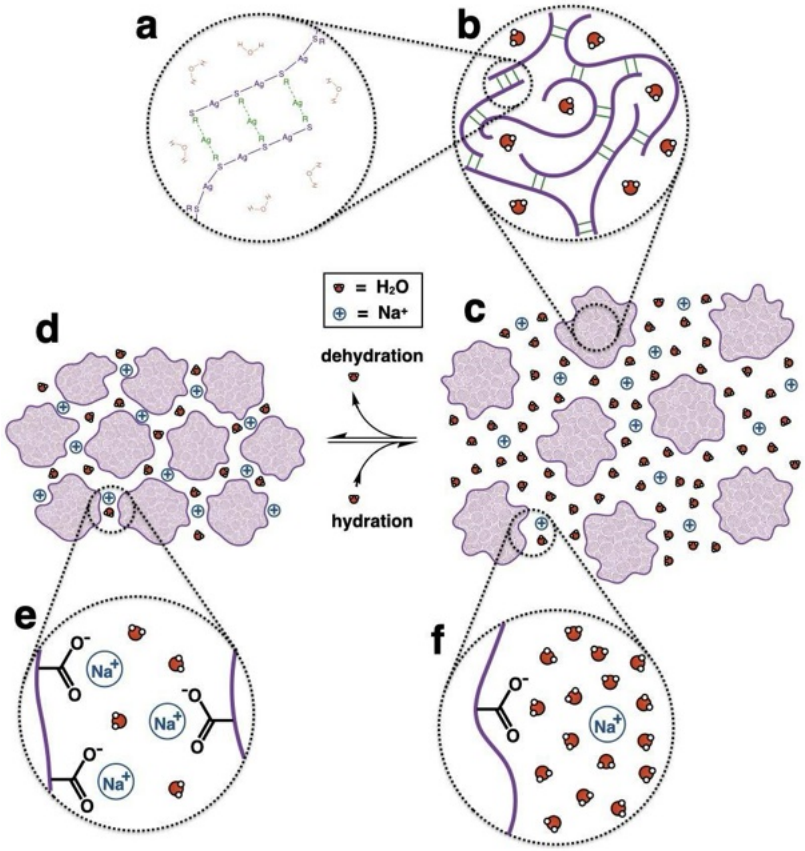

Figure 5: Scheme of RAMETRIC structure and method of agglomeration.

a) Molecular structure of linear silver-cysteine oligomers (purple) bridged through cysteine side chains by free Ag^+ ions (green). b) Illustration of silver-thiolate oligomers (purple lines) bridged by Ag^+ (green lines). c) colloidal sol containing flexible, globular colloids solvated by water with aqueous Na^+ ions. d) Dehydration drives the reversible sol-RAMETRIC transition as colloids agglomerate and trap Na^+ ions. The flexible colloids are expected to alter their shape to minimize void space. e,f) Insets of interstitial space between colloids in the e) RAMETRIC state, where Na^+ binds to cysteine's carboxylic acid functional groups, and f) sol state, where aqueous Na^+ ions are freely soluble.